Compact Chipless RFID Sensor for Frozen Food Monitoring

Cong Danh Bui, *Graduate Student Member, IEEE*, Aidan Quinn, *Senior Member, IEEE*, Daniela Iacopino, *Senior Member, IEEE*, and Adam Narbudowicz, *Senior Member, IEEE*

***Abstract*—Chipless RFID sensor is currently one of the most promising sensor designs, especially in food safety sector, because it has a robust structure and is inexpensive for mass production. This article proposes a simple, compact, and low-cost chipless RFID sensor tag for frozen food monitoring. The system consists of an interrogator antenna, which is an antipodal Vivaldi antenna, and a chipless RFID sensor tag inside a flat container that contains a small quantity of ice. When receiving power from the interrogator antenna, the sensor alters the frequency of the reflected signal if the ice melts. One of three states of the material in the container can be detected, i.e., ice, water, and air (empty container). The peak of the frequency response exhibits distinctively narrow 3-dB bandwidth of 35–49 MHz, allowing multiple sensors to operate simultaneously within limited bandwidth and space; peak center frequency is observed at 751 or 838 MHz, for, respectively, ice and air, with no peak present for water. The system is simulated, analyzed, and verified by measuring in free open space in a realistic environment. The measurement for ice melting over time is also measured and shown that frequencies of the peaks are slowly decreasing during the first 10 min after defrost and completely disappears after 15 min. The resonant peak reappears at 826 MHz after the tag is completely dry. A good tolerance to the background is also found when complex dielectric material is placed next to the sensor.**

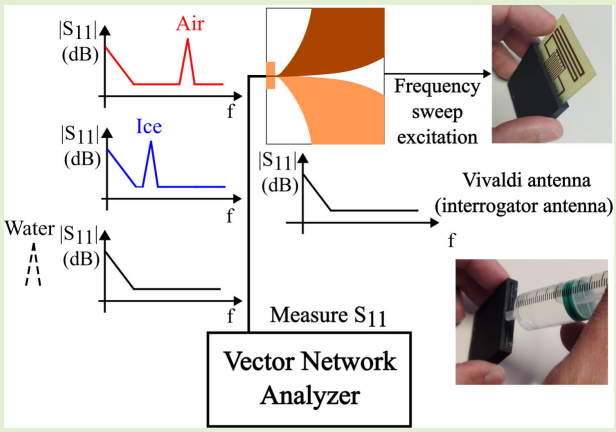

***Index Terms*— Antenna miniaturization, chipless RFID, cold chain integrity, permittivity sensing, sensors.**

I. Introduction

AROUND 17% amount of food is wasted in 2021 in household, food service, and retail and 14% of food production in the world is estimated to be lost during the supply chain, according to UNEP report [1]. Frozen food is a part of daily meals for millions of people around the world, especially in developing countries. Frozen food is convenient, easily accessible, has long best-before date and thus, reduce food waste around the world. Before reaching the intended customer, frozen food has to go through a chain of cold chain logistics and low temperature is one of the most important factors to extend the food's long shelf life as it prevents the bacteria from growing and spoiling the food [2].

Sensors are necessary to provide information about the quality of the food as well as environmental changes. Therefore, designing an efficient sensor for frozen food has been a focus of recent research. For example, a sensor was presented to monitor the freshness of fish by observing the color changes based on the pH level emitted [3]. On the other hand, toxins, such as Aflatoxins B1 or histamine in food, can be detected using multimode fiber and multicore fiber [4] or surface plasmon resonance [5], [6] in optical sensors, respectively. Light indicating and optical sensors to detect toxic elements have great practical applications. However, they did not address the challenges in the food industry, which are size reduction, low fabrication cost, and sensor robustness [7]. With wireless communication has become an essential part of modern technology, RFID sensors, which are tags from RFID technology, emerge as a promising candidate [8].

RFID tags are commonly categorized as chipped or chipless RFID tags. As the name suggests, a chipped RFID tag has a

Manuscript received 10 February 2024; revised 5 March 2024; accepted 13 March 2024. Date of publication 22 March 2024; date of current version 1 May 2024. This work was supported by the Science Foundation Ireland, under Grant 13/RC/2077_P2. The associate editor coordinating the review of this article and approving it for publication was Prof. Xingwang Li. *(Corresponding author: Adam Narbudowicz.)*

Cong Danh Bui is with CONNECT Centre, School of Engineering, Trinity College Dublin, The University of Dublin, D02 PN40 Dublin, Ireland (e-mail: buic@tcd.ie).

Aidan Quinn, Daniela Iacopino, and Adam Narbudowicz are with Tyndall National Institute, T12 R5CP Cork, Ireland (e-mail: aidan.quinn@tyndall.ie; daniela.iacopino@tyndall.ie; adam.narbudowicz@tyndall.ie).

Digital Object Identifier 10.1109/JSEN.2024.3378678

© 2024 The Authors. This work is licensed under a Creative Commons Attribution 4.0 License.
For more information, see https://creativecommons.org/licenses/by/4.0/

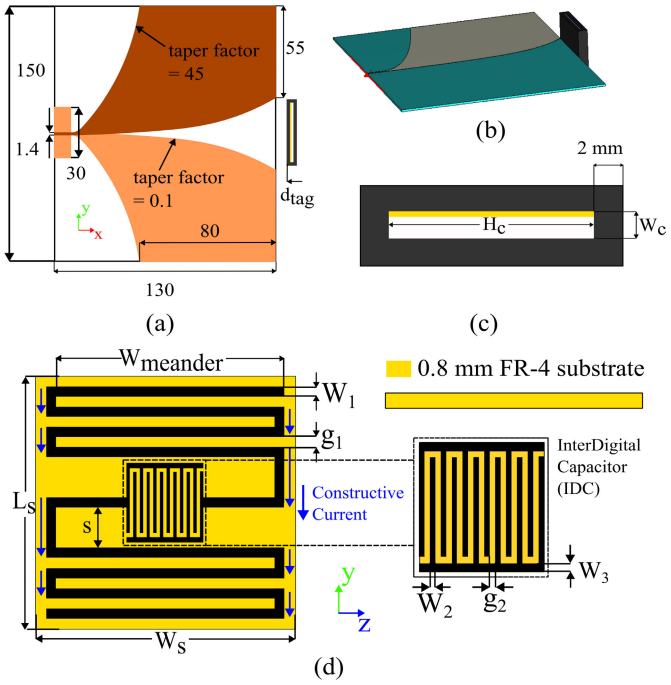

Fig. 1. Proposed design. (a) Vivaldi antenna—top view. (b) Vivaldi antenna—3-D view. (c) Container. (d) Proposed chipless tag design.

dedicated on-chip to read and transmit the stored information. There have been many sensors investigated to monitor the integrity of the cold chain. In [9], a temperature sensor using a dual-chip UHF tag was suggested. The design was made from shape-memory alloys, which is a temperature-sensitive material, to operate at low (0 °C) and high (80 °C). On the other hand, an RFID reader was used to record the received signal strength indicator to monitor the frozen meat temperature in an uncontrolled environment in [10]. Alternatively, a failure of the cold chain during transportation can be informed by modifying the RFID tag with a copper-doped ionic liquid [11]. The mechanism is based on the irreversible melting of the copper-doped liquid (8 °C) leading to the RFID tag state's transition. However, for simplicity and environmental footprint, many researchers focus on the chipless solution, which can significantly reduce fabrication process and cost, despite the fact it often leads to reduced performance [8]. In [12], a chipless pH-sensor design was suggested to detect meat freshness based on changes in frequency using pH-sensitive material on the resonant structure. On the other hand, the work in [13] investigated the dips in reflection coefficient and its complex performance of the unique composition of oil over wide frequency bandwidth (3–5 GHz).

In this article, we propose a chipless RFID permittivity-based sensor for frozen food storage monitoring. Different from previous publications, the proposed design does not require any special material or sophisticated calculations. The temperature change (i.e., whether the sample was frozen or the cold chain has been broken) is indicated by the resonant frequency, controlled by the permittivity of material under test (MUT) present in a small container attached to the tag. The miniaturization technique is used, which provides the electrically smallest sensing tag available in the literature, measuring only $0.1\lambda_0$ (3.5 cm at 800 MHz). This miniaturization also results in narrow bandwidth, which obtained from S_{11} of the Vector Network Analyzer attached to the interrogator antenna, of 79 MHz ($Q = 10$) and 59 MHz ($Q = 14$) with peak values of -2.9 and -2.7 dB when containing ice and air. The proposed design does not aim to identify the surrounding temperature but rather shows the necessary information in the cold-chain application, which is whether the ice is melting or not. The sensor utilizes the permittivity of ice (3.2), which is significantly lower than that of water (81), to identify whether the ice has melted or not. Specifically, if the temperature is consistently maintained low for ice formation, the frequency peak will be around 722–751 MHz. However, if the ice is melting, which leads to higher overall effective permittivity inside the container, the resonant peak on the Vivaldi antenna will be lower than 722 MHz. However, the frequency response is around 816–838 MHz meaning that the container is almost empty. The application is aimed toward monitoring frozen food, i.e., detecting breaks in cold-chain that can cause defrost and food spoilage. The sensor also shows a good tolerance toward background scatterers.

II. Proposed Design

Fig. 1 illustrates the proposed design of the tag [Fig. 1(d)] and antipodal Vivaldi antenna used as an interrogator. The interrogator antenna in Fig. 1(a) is designed on TMM10 substrate ($\varepsilon_r = 9.2$, $\tan\delta = 0.0022$ and 1.27 mm thick). The container box is 3-D printed with 2 mm thick of PLA material ($\varepsilon_r = 3.11$ and $\tan\delta = 0.013$) [14]. The box has an empty cavity of $35 \times 35 \times 2$ mm^2, which is initially filled with ice and the proposed chipless tag inside. The chipless tag is milled on low-cost FR-4 substrate ($\varepsilon_r = 4.3$, $\tan\delta = 0.025$ and 0.8 mm thick) due to easy fabrication process.

The Vivaldi antenna is the interrogator antenna for the proposed chipless tag. It offers stable gain and smooth frequency response without resonant behavior. Its planar structure simplifies the fabrication process and is more compact and cost-efficient than bulky horn antennas. It should be noted that—in general terms—any directional antenna covering the desired frequencies can be used in this role. However, an antenna exhibiting strong resonant behavior might require additional calibration, e.g., to avoid the case when the resonance of the tag is aligned with antenna's resonance. The Vivaldi antenna, due to its non-resonant radiating mechanism, eliminates this need, becoming a convenient interrogator. Its radiated signal couples into the tag in the near-field, then the reflected signal is frequency-modulated based on the material inside the 3-D-printed box toward the interrogator antenna and shown on S_{11} of Vector Network Analyzed attached to the antenna. The operation of the proposed design can be described as a block diagram in Fig. 2. By having multiple dielectric mediums, e.g., MUT, 3-D-printed box, the reflection of electromagnetic wave from the interrogator antenna is the culmination of multiple interactions. The most notable is the appearance of air impedance when separating the tag from the Vivaldi antenna, which has a major impact on both frequency

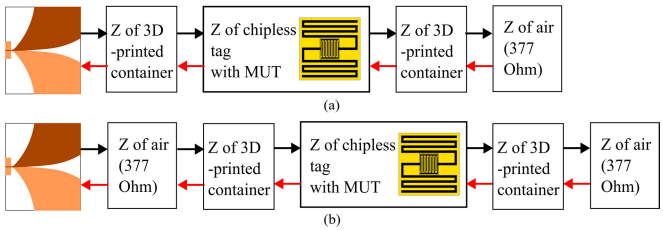

Fig. 2. Block diagram of the proposed design. (a) When $d_{tag} = 0$. (b) When separating d_{tag}.

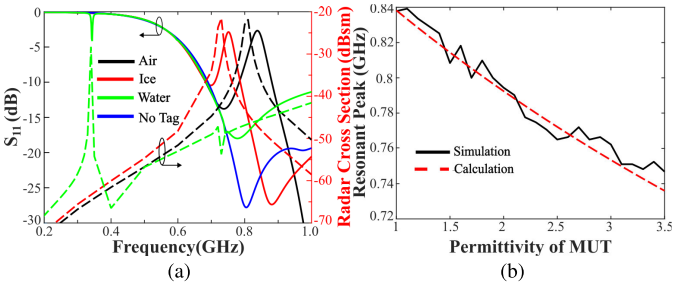

Fig. 3. (a) Reflection coefficient and RCS of the proposed system. (a) Air, ice, water, and no tag. (b) Frequencies of resonant peaks when changing permittivity of MUT.

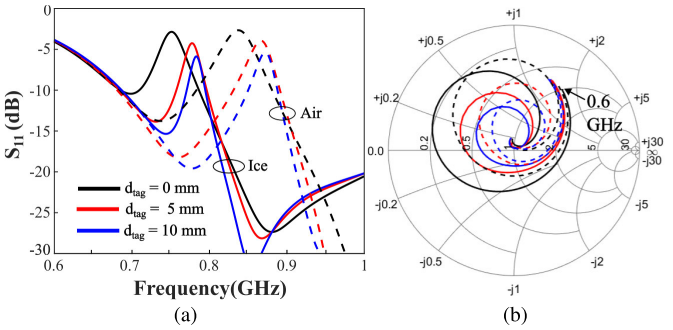

Fig. 4. (a) Reflection coefficient. (b) Impedance of the proposed system when changing d_{tag}.

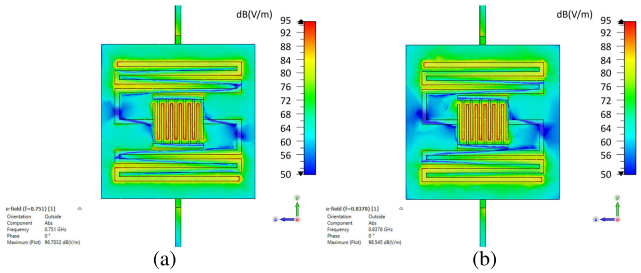

Fig. 5. Electric field distribution of the proposed system in (a) ice at 751 MHz and (b) air at 838 MHz (3-D-printed container is hidden for better visualization).

and magnitude of resonant peaks and will be discussed in Section III.

The sensor design is inspired by the miniaturized meander line dipole antenna. A classical dipole usually has the size of half-wavelength at its resonant frequency [15]. However, at 800 MHz, a half-wavelength dipole would be approximately 19 cm long, which is too large for practical applications. One of the most popular solutions is miniaturization by meandering the length of the dipole. The total length reduction can vary from 25% to 40% [16] based on multiple parameters, such as the linewidth, the gap between the meander lines, and the width of meandering. The miniaturization process always results in reduced bandwidth, due to increased amounts of stored energy in proportion to the radiated energy, and consequently increased Q-factor. This is known as the Chu-Harrington limit [17]. In the proposed sensing application, the narrow bandwidth is desirable, as it offers increased sensitivity due to distinct resonant frequency peak. As the peak is very frequency selective, it is unlikely to be misinterpreted with a scattering from natural objects in the proximity of the sensor.

The meander line tag has short connecting strips forming constructive currents because they are in phase while the ones along the $W_{meander}$ are destructive as they have opposite flow [18]. Therefore, despite not having the RF source in the middle as in the conventional design, it is important that the electric field of the interrogator antenna, which is created from its aperture, is the same as the constructive current so that the meander line resonator can be fully activated and create a clear resonant peak on S_{11} of Vivaldi antenna. Meanwhile, the main advantage of interdigital capacitor (IDC) is that its finger creates a long capacitive gap in a small area and it can be considered as a capacitor lump element. Parameters of the tag are as follows (all in mm) $W_s = 35$, $L_s = 35$, $W_1 = 1$, $g_1 = 1$, $s = 6$, $W_2 = 0.5$, $g_2 = 0.5$, $W_3 = 1$, $W_{meander} = 26.8$.

III. Analysis

The tag is a miniaturized meandered dipole loaded with an IDC. Because the MUT serves as a substrate for the dipole, the tag exhibits two different and distinct resonant frequencies, depending on whether the MUT is ice or air. Since ice has much higher permittivity than the air, it results in higher capacitance, thus lowering the peak resonant frequency of the dipole. Fig. 3(a) shows the simulation of the proposed antenna for four cases, where the container with MUT is filled with ice ($\epsilon = 3.2$) [19], water ($\epsilon = 81$) [20], or air ($\epsilon = 1$), as well as the case where there is no tag at all. All resonant peaks of air, ice, and water can be found at 810, 730, and 340 MHz, respectively, from radar cross section (RCS) by using an ideal plane-wave excitation using CST STUDIO. However, when using a realistic source from the Vivaldi antenna, the center resonant frequencies for ice and air are 751 and 838 MHz, respectively, while water shows no peak of reflection coefficient within the investigated band because the resonant frequency of water is much lower than the lower cut-off frequency (where $S_{11} < -10$ dB) of the interrogator antenna. Because the MUT can be seen as a superstrate of the tag, the initial estimation of the change in resonant frequency can be calculated as follows:

$$f_0 = \frac{c}{2L_{\text{eff}}\sqrt{\epsilon_{\text{eff}}}} \tag{1}$$

where c is the speed of light in vacuum (i.e., 3×10^8 m/s) and L_{eff} is the referenced effective length of the meander line. Effective permittivity is estimated as an average between the permittivity ϵ_{PLA} of the PLA container, the permittivity ϵ_{FR4} of the substrate board, and the permittivity ϵ_{MUT} of the MUT,

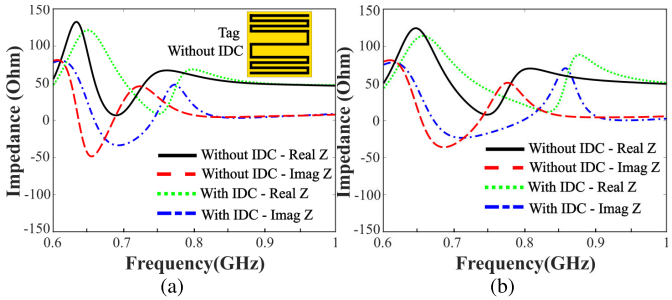

Fig. 6. Impedance of the proposed design with and without IDC. (a) Ice. (b) Air.

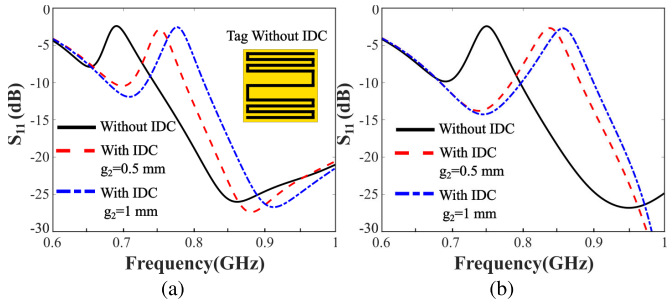

Fig. 7. Reflection coefficient of the proposed tag with and without IDC. (a) Ice. (b) Air.

i.e.,

$$\epsilon_{\text{eff}} \approx (\epsilon_{\text{PLA}} + \epsilon_{\text{FR4}} + \epsilon_{\text{MUT}})/3. \tag{2}$$

Since the total length of the meander line is about 267 mm, 40% size reduction is found to be the best match with the simulation results while also being in accordance with values reported in [16]. The general trend of resonant peaks is decreasing as the permittivity of MUT gets higher despite of some irregularities [Fig. 3(b)]. As a result, the proposed tag can distinguish between three different states of MUT, which usually occur in cold chain applications.

The distance parameter, d_{tag}, indicates the distance between the interrogator antenna and the tag. As shown in Fig. 4(a), the notches' magnitude gradually decreases when d_{tag} increases, also with a small frequency shift. This is most likely due to the coupled power from the interrogator antenna, which decreases as the distance d_{tag} increases. Since the tag is in the reactive near-field region of the Vivaldi antenna (i.e., $<$60 mm), the impedance seen at the Vivaldi antenna is, in fact, a combination of two contributors: the near-field effect of the distance d_{tag}, i.e., free-space distance over which the signal is transmitted and reflected back, and the impedance of the tag [Fig. 4(b)]. This means that the distance d_{tag} of this gap effectively acts as a form of impedance transformer, resulting in different impedance seen for different distances and consequently minor shifts in frequency response. It should be, however, noted that such minor shifts are significantly smaller than the frequency shifts caused by permittivity change of investigated MUTs and do not jeopardize the sensory role of the tag. When the antipodal Vivaldi antenna is placed next to the sensor, i.e., $d_{\text{tag}} = 0$ mm, the power received by the tag is the highest. However, with increased distance, the coupled power is reduced and also affected by the free space impedance and reactive effect in the near-field region of the Vivaldi antenna. Fig. 5 shows the electric field distribution of the tag at two frequencies: 751 MHz with the container filled with ice; and 838 MHz with the empty container. A strong electric field around the meander line tag is observed at two frequency responses (751 and 838 MHz) when MUT is ice and air, respectively.

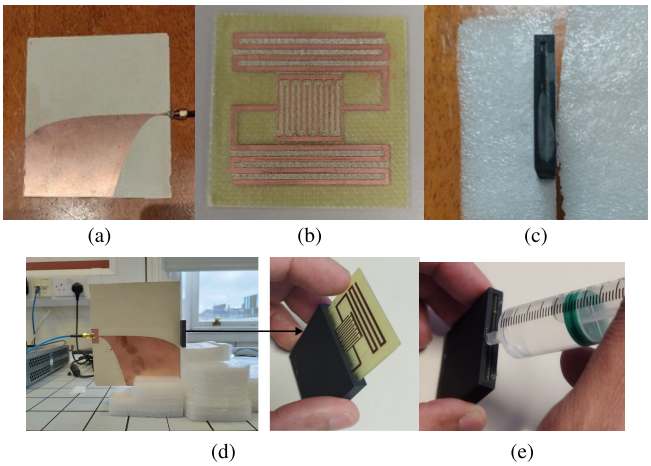

Fig. 8. Prototype of the proposed system. (a) Interrogator antenna. (b) Chipless RFID tag. (c) Three-dimensional printed box with chipless tag (d) Measurement setup. (e) Filling the container with distilled water to create ice MUT in a freezer.

The IDC, placed in the center of the meander line antenna, is considered as a lump element structure with multiple long conductive strips with small gap [21]. Simulation model of the proposed tag without IDC and with two different dimensions of IDC was performed. The IDC has a major impact on the impedance of the proposed design. Based on Fig. 6, while the overall impedance shifts from 7.9 + 18.5i Ω to 40.82 – 17i Ω when adding IDC, it also increases the resistance. It should be noted that the resonant peak of the proposed design is created by the impedance mismatch, i.e., the local minimum of the overall impedance. By introducing IDC, the resistance and admittance are shifted to a higher spectrum, thus increasing the resonant frequency. In addition, the rotation of IDC in the chipless RFID sensor has little effect on the overall performance of S_{11}. This is because at the used frequency the IDC is significantly smaller than the wavelength, and thus can be approximated as a lumped component. The IDC is used as a capacitive loading of the electrically small, meandered dipole antenna. Nevertheless, according to Fig. 7, the gaps g_2 of IDC not only help increase the frequency of resonant peaks but also widen the difference between two operating frequencies for ice and air, allowing more precise measurement. The difference is found to improve from 60 MHz (without IDC) to 86 MHz, which increases about 43% if using smaller gap g_2 of 0.5 mm in IDC. Therefore, parameter g_2 is 0.5 mm due to limitation in fabrication process.

IV. Experimental Results

Fabricated interrogator antenna, chipless tag, the MUT container box with the tag inside, and the complete measurement

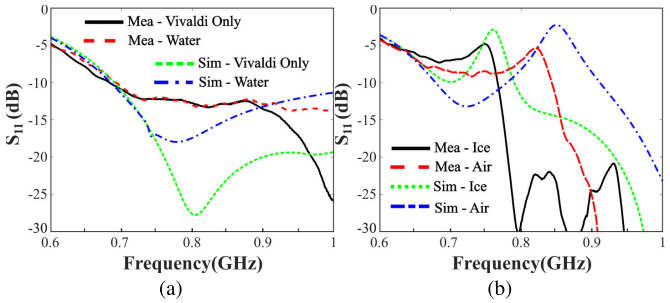

Fig. 9. Measurement of the proposed tag. (a) Water and only integrator antenna. (b) Ice and air.

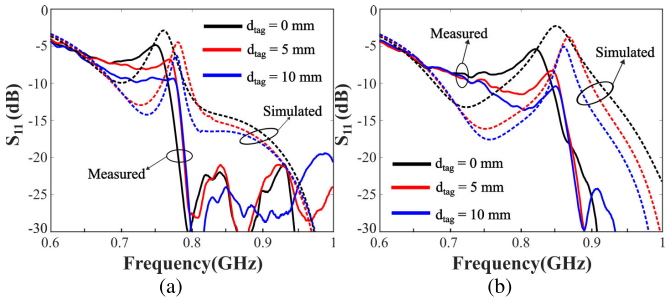

Fig. 10. Measurement of the proposed tag when changing d_{tag}. (a) Ice. (b) Air.

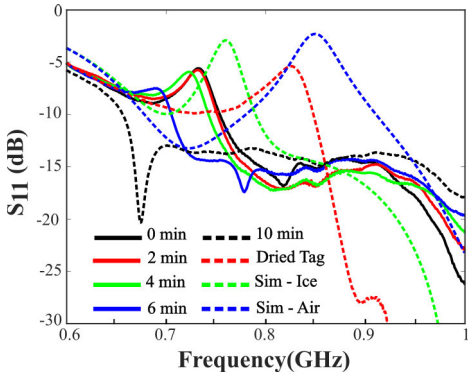

Fig. 11. Measurement of the proposed tag over time.

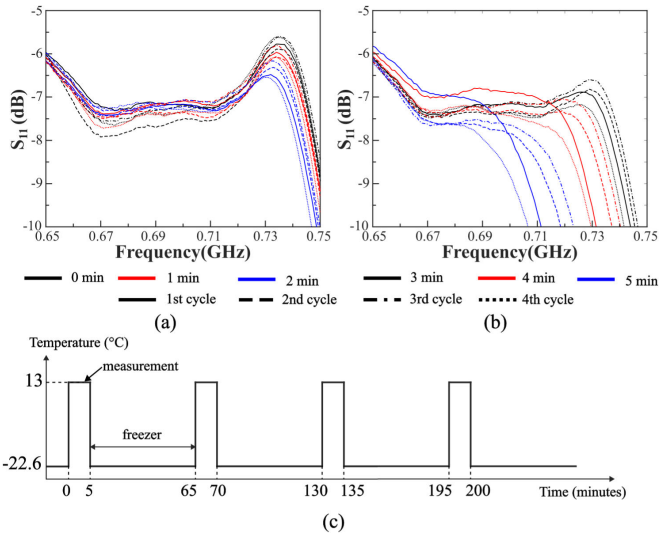

Fig. 12. Measurement of the proposed tag over time with a consistent temperature of 13 °C (a) 0–2 min, (b) 3–5 min, and (c) temperature profile during the measurement.

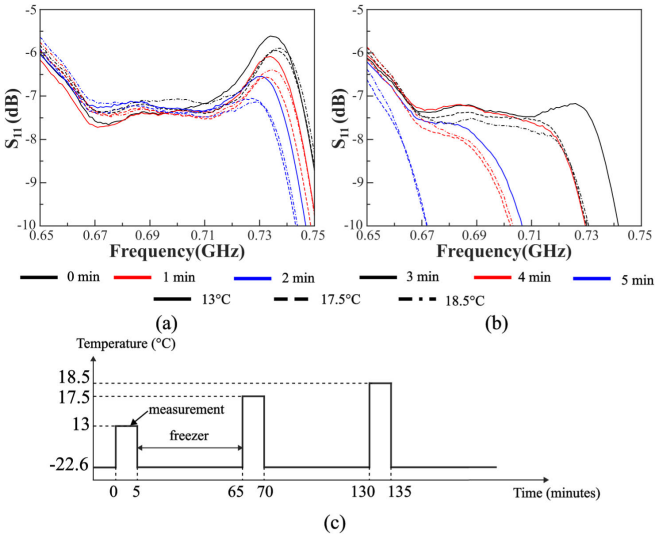

Fig. 13. Measurement of the proposed tag over time with increasing temperature (a) 0–2 min, (b) 3–5 min, and (c) temperature profile during the measurement.

setup are shown in Fig. 8. The ice MUT is created by filling the container with distilled water and placing in a freezer for 6 h (−22 °C). The setup is measured for the four simulated states, i.e., ice, water, air, and 'no-tag' case. As seen in Fig. 9, the $|S_{11}|$ shows resonant peaks for both ice and air while no peaks for water and only the interrogator antenna, as required to identify the melting. According to Fig. 10, the results exhibit lower magnitude and resonant frequencies, which is about 10 MHz/2 dB for ice and 30 MHz/3 dB for air when the interrogator antenna is placed directly next to the tag. This is most likely due to the background scatterers and variation in ice samples, as the measurements were conducted in regular office space (i.e., to mimic a realistic environment given the intended application), whereas simulations assumed perfect open space and perfect material. Nevertheless, the frequency change between the investigated cases is significantly greater than the discrepancy between simulation and measurement results, thus making the proposed technique still useful. For the distance $d_{\text{tag}} = 10$ mm, the magnitude of the measured resonant peaks of ice and air decreases to −9.4 and −10.4 dB, respectively, compared to −6.3 and −5.1 dB of those in simulation. This is most likely due to additional losses. Overall, the trend of the curves is the same as the ideal simulated predictions and the resonant frequencies for detecting both ice and air are clearly distinguishable.

Fig. 11 shows the change in measured reflection coefficient as a function of time, where $t = 0$ is the moment the tag is removed from the freezer into the room temperature environment of 13 °C (i.e., break of the frozen chain). During the first 15 min, the resonant peak is slowly moving toward lower frequency, with simultaneously decreasing amplitude, i.e., 724 MHz/−5.9 dB at 4 min and 691 MHz/−7.5 dB at 6 min. This is attributed to the higher permittivity and greater losses of distilled water, once the ice melts inside the

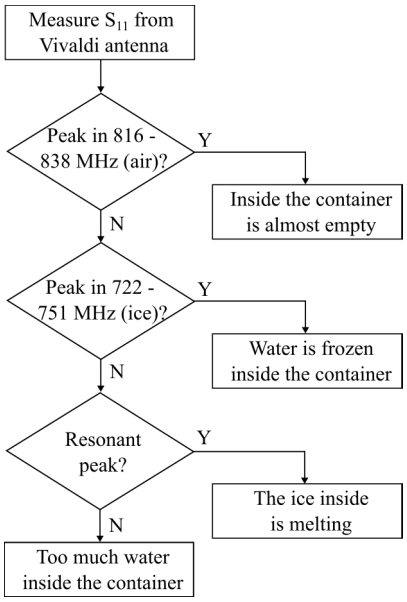

Fig. 14. Flowchart of the proposed design when measuring S_{11}.

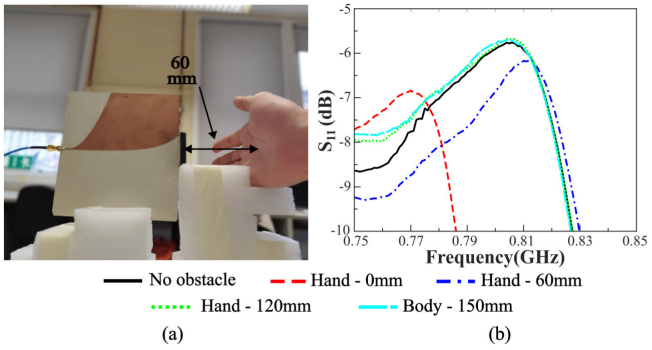

Fig. 15. Measurement of the effect of hand and human body. (a) Measurement setup. (b) S_{11}.

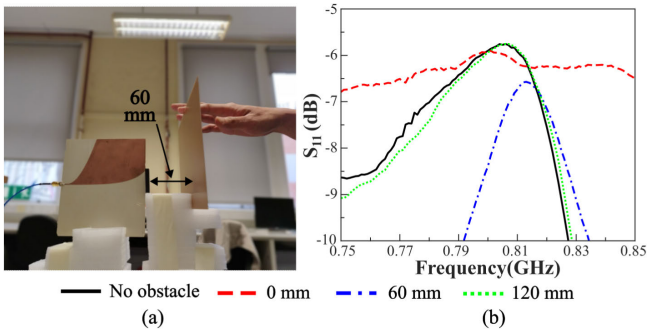

Fig. 16. Measurement of the effect of copper plate. (a) Measurement setup. (b) S_{11}.

container. After 6 min, as distilled water is still present inside the container, no frequency notches can be found until after four days, i.e., when the container box is completely dried out. The measured peaks are found closest to simulated ones after ten days, at 826 MHz with a magnitude of −5.4 dB. Within this time no interventions, such as drying with cloth or hot-air, was made to the tag.

To ensure the accuracy, repeatability, and reliability, the proposed sensor was measured over time six more times, where S_{11} is recorded every 1 min for 5 min. Except for the initial cycle, when the MUT is left in the freezer overnight, all five consecutive cycles were separated by 1 h in the freezer (−22 °C) to refreeze the tag and MUT. In other words, after taking out of the freezer, the tag was placed next to the interrogator antenna and measured continuously for 5 min before putting it back in the freezer again. During the first four cycles, the temperature of the room is kept around 13 °C. For repeatability, the tag was secured so that the melted water stayed within the MUT container. This is different from typical operation, when the water is allowed to leak out in order to detect re-freezing cycles. According to Fig. 12, in all four attempts, the magnitude of the resonant peaks has a slight discrepancy of less than 1 dB while its frequencies show little to no changes up until 3 min of recording. After 4 and 5 min, water droplets can be found visibly and the peaks started to disappear. In the next two attempts, we increased the environmental temperature (Fig. 13). The magnitude of the peak was decreasing at a much faster rate compared to Fig. 12. There were no resonant peaks that can be found after 3 min in higher temperatures, i.e., 17.5 °C and 18.5 °C.

The proposed sensor does not aim to measure the exact temperature but rather to detect the appearance of water, which is a sign of a cold chain break. By referencing the current resonant peak with that of ice and air, one can know whether the ice is melting or not (Fig. 14). If the resonant frequency is lower than 751 MHz (ice) but the peak is still visible, it indicates the ice started melting. However, no peaks in S_{11} indicate significant amounts of water in the MUT, which is equivalent to the break of the cold chain. On the other hand, the occurrence of the frequency peak between 816 and 838 MHz implies that MUT is air, i.e., neither ice nor water present. The melting rate can be different based on the humidity and temperature of the surrounding environment.

All measurements are performed in a regular office setting and the effect of surrounding obstacles is also included. Various reference measurements are performed when the MUT container is empty. The results for ice and water follow a similar trend. While there are numerous dielectric obstacles available, the human body and body parts are the most common. Fig. 15(a) shows the measurement setup when placing a hand behind the sensor (an example of 60 mm) in an office room. According to Fig. 15(b), the hand has a small impact to the frequency peak of about 40 MHz/1 dB if placed next to the sensor. The hand's impact gradually decreases when increasing the distance and even a full human body has little effect on the resonant frequency.

Fig. 16(a) illustrates a case, when a copper plate of 15 × 23 cm^2 is placed 60 mm behind the sensor. Fig. 16(b) indicates that the resonant peak appears again after increasing the distance between the copper and the Vivaldi antenna to 60 mm. The undesired impact is not visible when the distance to the plate is 120 mm or more. The copper plate next to the sensor acts as a ground plane in the near field, thus altering tag's resonant performance. On the contrary, for the human body, the dominating phenomena is absorption into the lossy and complex dielectric material—hence smaller effect on the reflected signal.

TABLE I
COMPARISON OF THE PROPOSED DESIGN WITH RECENT WORKS

Ref	Resonator & f_c (GHz)	Result	Size (λ_c^2)	Sensing Parameter	Sensitivity
[22]	ELC[1](3.95) CSRR[2](3.26)	S_{21}	0.5x 0.6	Temperature & Humidity	2.18 MHz/RH 898.63 MHz/°C
[23]	U & L-shape resonator (7)	RCS	0.4x 0.6	Temperature & Crack	-58.8 MHz/0.1mm 2.62 MHz/°C
[24]	2 circular SRR[3](6.45)	S_{21}	0.5x 0.5	Temperature	0.475 MHz/°C
[25]	C-scatterer (5.85)	RCS	1.6x 0.5	Temperature	0.1 MHz/°C
[13]	CASRR[4] (3-5)	S_{11}	0.5x 0.5	Temperature	14.2,17.3, 23.6°C in 3 oil types
[12]	Dipoles with pH-sensitive material (0.8)	S_{11}	>0.3 x0.3	pH	20% frequency shift to detect spoilage
This work	Meander line (0.8)	S_{11}	0.1x 0.1	Temperature	2 resonant peaks for air and ice

[1] Electric field LC-coupled; [2] Complementary Split Ring Resonator; [3] Split Ring Resonator; [4] Circular Asymmetric Split Ring Resonator

The comparison of the proposed design with recent work on chipless RFID sensors is shown in Table I. In most of the recent designs, an intermediate step is required to analyze the measured results with reference one to obtain the sensing parameter. In [22] and [23], the sensors were designed to be able to sense multiple environment parameters with small shift in resonant frequency. Dedicated temperature sensors in [24] need two antennas for S_{21} result and in [25] requires RCS measurement, which is not preferred outside of controlled environment and desires of target calibration [26]. Chipless sensor using S_{11} is easier to measure but the temperature sensor in [13] depends on a more extensive analysis of unique signal response changing from solid to liquid state and pH sensor in [12] demands two resonators, where one has a layer of pH-sensitive material, to observe the spectral shift. However, the proposed sensor took a more direct approach with S_{11} on a single antenna. The frequency shift from 838 to 751 MHz can be observed, without comprehensively analyzing within a full wideband spectrum. Further observation of the resonant peaks can show whether the ice is melting (i.e., the peak frequency is lower than that of ice) or having little water inside (i.e., the peak frequency is between that of ice and air state). Additionally, the proposed sensor is the smallest in terms of wavelength compared to other works, which makes it easily implemented on many applications.

V. CONCLUSION

The work proposed a simple chipless sensor for monitoring breaks in frozen food storage. The break in the cold chain, e.g., ice is melting, can be easily detected by observing resonant peaks in S-parameters of antipodal Vivaldi antenna, which are 751 MHz for ice, 838 MHz for air, and no peaks for water. The goal of the proposed sensor is to detect cold chain break, which usually happens when there is water inside the container, by observing the resonant peaks in S_{11} from interrogator antenna. Additionally, the resonant peaks only have minor shifts even when placing a human hand next to the sensor and thus, demonstrating little sensitivity to the background of the sensor. Compared to previously published designs, the proposed chipless tag is low-profile, small, and easily printable as well as does not require any complicated formulas or analytical procedure, which is an advancement in sensor design for cold chain application. The sensor is also found to have good tolerance to the background when there is little shift in resonant peaks.

REFERENCES

[1] (2021). *UNEP Food Waste Index Report 2021*. Accessed: Jan. 1, 2024. [Online]. Available: https://www.unep.org/resources/report/unep-food-waste-index-report-2021

[2] J. A. Evans, *Frozen Food Science and Technology*. Hoboken, NJ, USA: Wiley, 2009.

[3] M. Moradi, H. Tajik, H. Almasi, M. Forough, and P. Ezati, "A novel pH-sensing indicator based on bacterial cellulose nanofibers and black carrot anthocyanins for monitoring fish freshness," *Carbohydrate Polym.*, vol. 222, Oct. 2019, Art. no. 115030.

[4] X. Liu et al., "Plasmonic sensor based on offset-splicing and waist-expanded taper using multicore fiber for detection of Aflatoxins B1 in critical sectors," *Opt. Exp.*, vol. 31, no. 3, pp. 4783–4802, 2023.

[5] W. Zhang, R. Singh, F.-Z. Liu, C. Marques, B. Zhang, and S. Kumar, "WaveFlex biosensor: A flexible-shaped plasmonic optical fiber sensor for histamine detection," *IEEE Sensors J.*, vol. 23, no. 19, pp. 22533–22542, Oct. 2023.

[6] P. S. Pandey, S. K. Raghuwanshi, and S. Kumar, "Recent advances in two-dimensional materials-based Kretschmann configuration for SPR sensors: A review," *IEEE Sensors J.*, vol. 22, no. 2, pp. 1069–1080, Jan. 2022.

[7] P. Fathi, N. C. Karmakar, M. Bhattacharya, and S. Bhattacharya, "Potential chipless RFID sensors for food packaging applications: A review," *IEEE Sensors J.*, vol. 20, no. 17, pp. 9618–9636, Sep. 2020.

[8] N. C. Karmakar, E. M. Amin, and J. K. Saha, *Chipless RFID Sensors*. Hoboken, NJ, USA: Wiley, 2016.

[9] S. Caizzone, C. Occhiuzzi, and G. Marrocco, "Multi-chip RFID antenna integrating shape-memory alloys for detection of thermal thresholds," *IEEE Trans. Antennas Propag.*, vol. 59, no. 7, pp. 2488–2494, Jul. 2011.

[10] A. M. J. Marindra, B. M. Pratama, and D. J. Suroso, "Non-invasive frozen meat monitoring system using UHF RFID tag antenna-based sensing and RSSI," *Int. J. Adv. Sci., Eng. Inf. Technol.*, vol. 13, no. 1, pp. 1–7, Jan. 2023.

[11] F. Vivaldi et al., "A temperature-sensitive RFID tag for the identification of cold chain failures," *Sens. Actuators A, Phys.*, vol. 313, Oct. 2020, Art. no. 112182.

[12] J. Waimin et al., "Low-cost nonreversible electronic-free wireless pH sensor for spoilage detection in packaged meat products," *ACS Appl. Mater. Interfaces*, vol. 14, no. 40, pp. 45752–45764, Oct. 2022.

[13] F. Villa-Gonzalez, R. Bhattacharyya, T. Athauda, S. Sarma, and N. Karmakar, "Detecting breaks in cold chain integrity using chipless RFID time–temperature sensors," *IEEE Sensors J.*, vol. 22, no. 18, pp. 17808–17818, Sep. 2022.

[14] B. Behzadnezhad, B. D. Collick, N. Behdad, and A. B. Mcmillan, "Dielectric properties of 3D-printed materials for anatomy specific 3D-printed MRI coils," *J. Magn. Reson.*, vol. 289, pp. 113–121, Apr. 2018.

[15] C. A. Balanis, *Antenna Theory: Analysis and Design*. Hoboken, NJ, USA: Wiley, 2016.

[16] J. Rashed and C.-T. Tai, "A new class of resonant antennas," *IEEE Trans. Antennas Propag.*, vol. 39, no. 9, pp. 1428–1430, Sep. 1991.

[17] J. S. McLean, "A re-examination of the fundamental limits on the radiation Q of electrically small antennas," *IEEE Trans. Antennas Propag.*, vol. 44, no. 5, p. 672, May 1996.

[18] M. El Atrash, M. A. Abdalla, and H. M. Elhennawy, "Gain enhancement of a compact thin flexible reflector-based asymmetric meander line antenna with low SAR," *IET Microw., Antennas Propag.*, vol. 13, no. 6, pp. 827–832, May 2019.

[19] R. Kozak, B. D. Wiltshire, M. A. R. Khandoker, K. Golovin, and M. H. Zarifi, "Modified microwave sensor with a patterned ground heater for detection and prevention of ice accumulation," *ACS Appl. Mater. Interfaces*, vol. 12, no. 49, pp. 55483–55492, Dec. 2020.

[20] H. Griffiths, W. Gough, S. Watson, and R. J. Williams, "Residual capacitive coupling and the measurement of permittivity in magnetic induction tomography," *Physiolog. Meas.*, vol. 28, no. 7, pp. S301–S311, Jul. 2007.
[21] R. Beeresha, A. Khan, and H. Manjunath-Reddy, "Design and optimization of interdigital capacitor," *Int. J. Res. Eng. Technol.*, vol. 5, no. 21, pp. 73–78, 2016.
[22] L. Liu and L. Chen, "Characteristic analysis of a chipless RFID sensor based on multi-parameter sensing and an intelligent detection method," *Sensors*, vol. 22, no. 16, p. 6027, 2022.
[23] N. Javed, M. A. Azam, and Y. Amin, "Chipless RFID multisensor for temperature sensing and crack monitoring in an IoT environment," *IEEE Sensors Lett.*, vol. 5, no. 6, Jun. 2021, Art. no. 6001404.
[24] B. Wang, Y. Li, and T. Gu, "Design of a metamaterial chipless RFID sensor tag for high temperature," *AIP Adv.*, vol. 13, no. 3, Mar. 2023, Art. no. 035218.
[25] H. El Matbouly, S. Tedjini, K. Zannas, and Y. Duroc, "Compact multi bit slotted C-Scatterer for threshold sensitive chipless wireless temperature sensor," *Technologies*, vol. 6, no. 3, p. 59, Jun. 2018.
[26] K. R. Brinker, M. Vaccaro, and R. Zoughi, "Application-adaptable chipless RFID tag: Design methodology, metrics, and measurements," *IEEE Trans. Instrum. Meas.*, vol. 69, no. 6, pp. 3882–3895, Jun. 2020.

Cong Danh Bui (Graduate Student Member, IEEE) was born in Ho Chi Minh, Vietnam, in 1996. He received the B.S. degree from Ho Chi Minh University of Technology, Ho Chi Minh, in 2018, and the M.S. degree from Ton Duc Thang University, Ho Chi Minh City, in 2021. He is pursuing the Ph.D. degree in CONNECT Center, School of Engineering, Trinity College Dublin, Dublin, Ireland.

During the M.S. degree, he was with Ton Duc Thang University, as a Research Assistant Designing and optimizing array antenna with metasurface, leaky wave, and reconfigurable antennas. His current topic of interest is designing chipless RFID tags as sensors for various applications.

Aidan Quinn, photograph and biography not available at the time of publication.

Daniela Iacopino (Senior Member, IEEE) received the master's degree in chemistry from Universitá di Pavia, Pavia, Italy, in 1995, and the Ph.D. degree in chemistry from Universitá di Modena, Modena, Italy, in 2000.

From 2000 to 2002, she was a Postdoctoral Fellow with the Department of Chemistry, University College Dublin, Dublin, Ireland. In 2002, she was moved to Tyndall (then NMRC) a Postdoctoral Fellow. Since 2006, she has been as a Senior Researcher with the Nanotechnology Group, Tyndall National Institute, Cork, Ireland. Since 2012, she has been leads the Integrated Nanomaterials (INMs) team, whose research focus on synthesis and integration of nanostructured materials into devices for sustainable sensing and energy storage applications. She is Funded Investigator in CONNECT and VistaMilk SFI Research Centre and has a long history of research funding including participation to national (SFI, EI, IRC) and international (EU FP6, FP7, H2020, HE21/22) frameworks both as partner and PI.

Adam Narbudowicz (Senior Member, IEEE) received the M.Sc. degree from Gdansk University of Technology, Gdansk, Poland, in 2008, the Ph.D. degree from Dublin Institute of Technology (now TU Dublin), Dublin, Ireland, in 2013, and the Habilitation (advanced doctorate) degree from Wroclaw University of Science and Technology, Wroclaw, Poland, in 2020.

He is currently a Senior Researcher with the Tyndall National Institute, Dublin, Ireland, and also a part-time Associate Professor with Wroclaw University of Science and Technology. He was previously as a Senior Researcher with Trinity College Dublin, Dublin, Ireland. He was a Postdoctoral Fellow of Marie Skłodowska-Curie Action co-funded projects, including (twice) of research stay at RWTH Aachen University, Aachen, Germany. He has authored or coauthored more than 90 scientific publications in journals and peer-reviewed conference proceedings. His research interests include antenna miniaturization and electrically small antennas, machine learning for remote sensing, and sustainable antenna technology.

Dr. Narbudowicz received number of awards and distinctions, including the Scholarship for the Outstanding Young Polish Scientists in 2019, the Inaugural 2018 Prof. Tom Brazil CONNECT Excellence in Research Award, the Best Poster at the 2018 IEEE-EURASIP Summer School on Signal Processing, the 3rd Best Paper Award during ISAP 2017. He was also a mentor to the Finalist Team of the 2020 IEEE APS Student Design Contest. He sits on the Management Committee of the COST Action SyMat: "Future communications with higher-symmetric engineered artificial materials." He serves as the Vice-Chair for the IEEE Poland APS/MTT/AES Joint Chapter and the Vice-Chair for the Small Antenna Working Group of The European Association on Antennas and Propagation (EurAAP).